SCIENCE CHINA
Chemistry

• ARTICLES •

HOT PAPER

doi: 10.1007/s11426-015-5474-y

What are the practical limits for the specific surface area and capacitance of bulk sp^2 carbon materials?

Yanhong Lu[1,2*], Guankui Long[2], Long Zhang[2], Tengfei Zhang[2], Mingtao Zhang[2], Fan Zhang[2], Yang Yang[2], Yanfeng Ma[2] & Yongsheng Chen[2*]

[1]*School of Chemistry & Material Science, Langfang Teachers University, Langfang 065000, China*
[2]*Key Laboratory of Functional Polymer Materials and Center for Nanoscale Science and Technology; Institute of Polymer Chemistry, College of Chemistry, Nankai University, Tianjin 300071, China*

Received May 11, 2015; accepted May 27, 2015

The possible practical limits for the specific surface area and capacitance performance of bulk sp^2 carbon materials were investigated experimentally and theoretically using a variety of carbon materials. We find the limit for the specific surface area to be 3500–3700 $m^2\ g^{-1}$, and based on this, the corresponding best capacitance was predicted for various electrolyte systems. A model using an effective ionic diameter for the electrolyte ions was proposed and used to calculate the theoretical capacitance. A linear dependence of experimental capacitance versus effective specific surface area of various sp^2 carbon materials was obtained for all studied ionic liquid, organic and aqueous electrolyte systems. Furthermore, excellent agreement between the theoretical and experimental capacitance was observed for all the tested sp^2 carbon materials in these electrolyte systems, indicating that this model can be applied widely in the evaluation of various carbon materials for supercapacitors.

graphene, bulk sp^2 carbon materials, supercapacitor, specific surface area, DFT modeling

1 Introduction

Due to their high porosity and specific surface area (SSA), bulk sp^2 carbon materials including the oldest activated carbons (ACs) and the newest graphene based materials have attracted increasing interest for various applications such as for high performance supercapacitors (SCs) [1–6]. Various strategies have been sought for increasing the SSA and controlling the pore size distribution (PSD) in order to enhance SC performance [7–13]. While bulk sp^2 carbon materials such as ACs have been used for many years in scientific community and for industrial applications, and various sp^2 carbon including carbon nanomaterials have been widely studied in the last few decades [14,15], it is still unclear what are the limits for the SSA and corresponding capacitance performance of bulk sp^2 carbon materials in practice.

In this work, a series of bulk sp^2 materials were prepared and a systematic experimental and theoretical investigation was carried out to study the possible practical limits in terms of the SSA and its corresponding best capacitance. In our approach, an effective ionic diameter (EID) model for the electrolyte ions was proposed and the theoretical capacitance (C_{th}) of a series of sp^2 carbon materials in different electrolyte systems was calculated. The resulting values are consistent with the experimental capacitance (C_{ex}). A general linear relationship between C_{ex} and the effective SSA (E-SSA) of the carbon materials is obtained in all the ionic liquid (IL), organic and aqueous electrolyte systems studied. Most importantly, both experimental and theoretical results suggest that the highest practical SSA for bulk sp^2 materials is about 3500–3700 $m^2\ g^{-1}$ and the corresponding best capacitance performance was predicted for various

*Corresponding author (email: luyanhong_2003@126.com; yschen99@nankai.edu.cn)

electrolyte systems.

2 Experimental

2.1 Synthesis of various bulk sp^2 carbon materials

The bulk sp^2 carbon materials were prepared by a modified procedure in our previous report [16], as detailed in the Supporting Information online. Briefly and as an example, a given mass of carbon source was first hydrothermally treated at 180 °C for 12 h to obtain the hydrothermal product, followed by a chemical activation step at 900 °C for 1 h using KOH as the activation agent and with the weight ratio of 4:1. Then the final products were obtained after thorough washing and vacuum drying. The series of products were denoted as follows. Using the phenol/formaldehyde (PF)/graphene oxide (GO) mixture as carbon source, when the weight ratio of PF to GO was 8:1, 16:1, 24:1, the products were named P@8GA, P@16GA, P@24GA, respectively. When other mixtures of GO were used as the carbon source, PVA/GO with the ratio of 20, sucrose/GO with the ration of 24, cellulose/GO with the ratio of 24 and lignin/GO with the ratio of 24, the corresponding products were denoted V@20GA, S@24GA, C@24GA and L@24GA, respectively. Products GA, BA and PA were obtained using GO, bitumen and the phenol/formaldehyde mixture as the carbon source respectively following the same procedure.

In order to obtain an as wide as possible distribution of SSA and pore size distribution of the products, different temperatures and activation parameters were used, with different activation agents CaO, H_3PO_4, $ZnCl_2$, K_2CO_3, NaOH and KOH, activation temperatures from 600 to 1100 °C, and ratios of activation agent to intermediate hydrothermal products from 8:1 to 2:1, as shown in Table S1 (Supporting Information online). Commercial activated carbon materials, RP20, GAC and HXAC were used directly as purchased without further treatment.

2.2 Characterization

The structures of the samples were investigated by X-ray diffraction (XRD) performed on a Rigaku D/Max-2500 diffractometer (Japan) with Cu Kα radiation. Raman spectra were examined with a LabRAM HR Raman spectrometer using laser excitation at 514.5 nm. The stack height (L_c) and lateral size (L_a) of the graphene domains were estimated from the XRD and Raman results, as detailed in the Supporting Information online. The nitrogen adsorption/desorption analysis was done at 77 K on a Micromeritics ASAP 2020 apparatus. The SSA was obtained by the Brunauer-Emmett-Teller (BET) method based on adsorption data in the relative pressure (P/P_0) range of 0.05 to 0.3. The PSD was analyzed using a nonlocal density functional theory (NL-DFT) method with a slit pore model from the nitrogen adsorption data [17,18].

2.3 Fabrication of SC and C_{ex} measurement

The SC cells of all the bulk sp^2 carbon materials were fabricated using a symmetrical two-electrode system with different sp^2 carbon materials following our previous work [19,20] and the recommended best practice for a reliable performance evaluation of materials for SC [21–23]. Briefly, 90 wt% active carbon material and 10 wt% binding agent PTFE were homogeneously mixed in an agate mortar. Then the mixture was rolled into 100–120 μm thickness sheets and punched into 13 mm diameter electrodes. After dried at 120 °C for 6 h under vacuum, the electrodes were weighted and hot pressed onto the current collectors (foils with conducting carbon coating or Ni foams) and then dried at 180 °C for 6 h under high vacuum. The dry electrodes were transferred into a glove box filled with Argon to construct the two-electrode symmetrical SC which consisted of two current collectors, electrolyte, two electrodes with identical weight and a porous cellulose separator sandwiched in a test fixture consisting of two stainless steel plates. The typical active material's weight is ~10 mg for one device (two electrodes). Different electrolyte systems including IL ($MMIMBF_4$, $EMIMBF_4$, $BMIMBF_4$, $HMIMBF_4$, $OMIMBF_4$ and $EMIMNTf_2$), organic electrolyte (1.0 mol/L $TEABF_4$/AN and 1.0 mol/L $TEABF_4$/PC) and aqueous (6 mol/L KOH) systems were investigated. The applied voltage windows were different depending on different electrolyte systems, which was 0–3.5 V for IL, 0–2.7 V for organic and 0–1.0 V for aqueous system, respectively.

For the experimental capacitance performance of the materials, Galvanostatic charge-discharge cycle tests were carried out using a battery test system (LAND CT2001A model, Wuhan LAND Electronics. Ltd., China) at a current density of 1.0 A g^{-1}. The specific capacitance C_p (F g^{-1}) of each sp^2 carbon materials in the symmetric SC was calculated according to the following equation:

$$C_p = \frac{4I}{m\mathrm{d}V/\mathrm{d}t} \quad (1)$$

where I is the constant current (A), m is the total mass (g) of the active materials on the two single electrodes, $\mathrm{d}V/\mathrm{d}t$ (V/s) is the slope obtained by fitting a straight line to the discharge curve over the range from V (the voltage at the beginning of discharge) to $V/2$.

2.4 Theoretical modeling and calculation

All DFT calculations were performed with the Gaussian 09 program package (Gaussian 09, Revision B.01, Wallingford CT: Gaussian, Inc., 2010, see Supporting Information online for full citation).

2.4.1 Construction of EID model and calculation of E-SSA and C_{th}

A general model for the EID was used for all the electrolyte ion size in different electrolyte systems. In pure IL electrolyte systems where there is no solvation, the EID was taken as the theoretical diameter of electrolyte ions obtained by using DFT calculations (B3LYP/6-31G*) [24,25] and the cation sizes of $EMIM^+$, $BMIM^+$ were 0.752 and 1.107 nm, respectively. When solvents were used together such as that in organic and aqueous electrolyte systems, a solvation shell was considered and added to the naked ion size to obtain the EID. With this model, the EIDs of 1.0 mol/L TEA^+ in organic solvent AN and 6 mol/L K^+ in water were taken as 1.320 and 0.662 nm, respectively, following the literatures [26–28].

The E-SSA, which is the effective accessible surface area for the electrolyte ions, was calculated using the cumulative DFT SSA, the PSD of the carbon materials and the electrolyte ion size. With the E-SSA, based on the EID of different electrolyte ions discussed above, the theoretical capacitance C_{th} was calculated for all the sp^2 carbon materials in various electrolyte systems. The detailed calculation process is shown in Tables S3–S6.

2.4.2 Calculation of the possible stable and smallest graphene sheet size and theoretical SSA

To obtain the possible stable and smallest graphene sheet (fragment) in theory, first the geometry optimization of all the graphene fragments with different sizes (carbon atoms) were performed at the B3LYP levels of theory with the 3-21G basis set [24,25]. The frequency analysis was employed at the same level of theory to check whether the optimized geometrical structures were at stable states and to evaluate the zero-point vibration energy (ZPE). With these graphene fragments, a thermodynamic calculation was used. The stable and smallest graphene fragment was then predicted under practical experimental conditions. More details for this part are in the Section 3 and the Supporting Information online.

With a given graphene sheets size, the theoretical SSA of the sp^2 carbon materials was calculated from a simple Monte Carlo integration technique where the probe molecule is "rolled" over the framework surface, and the probe radius is 1.82 Å (the kinetic radius of N_2) [29,30].

3 Results and discussion

3.1 The BET SSA of various bulk sp^2 carbon materials

In order to obtain the possible practical highest and widest range of SSA values, in addition to various carbon source materials, a wide range of preparation parameters was studied (Table S1). With these numerous experimental results using different carbon sources under different treatments, the best experimental BET SSA was obtained as >3500 $m^2\ g^{-1}$ for bulk sp^2 carbon materials.

The detailed morphology information of these bulk sp^2 carbon materials has also been carried out using XRD and Raman (Table S2). The average domain height L_c of the optimized activation products is found at 0.7–0.8 nm, and the approximate dimensional size is around 5×5–6×6 nm^2 depending on different carbon sources. These results suggest that the basic structure units in the high SSA sp^2 carbon materials are graphene sheets in the size of a few nanometers and most of which should be wrinkled single-layer sheets with likely some fewlayered, as observed before [16,31].

3.2 The E-SSA and theoretical capacitance performance in different electrolyte systems

Based on the various carbon materials prepared, the effective surface area, E-SSA, the area accessible to the electrolyte ions, was obtained from the overall SSA and PSD of the material and the electrolyte ion size [31] and C_{th} was then calculated. Note that for solvent free IL ions, C_{th} could be easily obtained as there is no solvation issue. But for aqueous and organic electrolyte systems, the ion size depends heavily on the solvation layer. With these in mind, a more general model was proposed, where the layers of solvent molecules around the ions were taken into account (Figure S1, Supporting Information online). Thus, the actual electrolyte ion size (EID), was obtained as the sum of the sizes of the naked ion and the shell of solvent molecules, following the literature [27,28]. Based on the EID model and the method in our previous work [31], the corresponding C_{th} of the prepared materials in several most widely studied electrolyte systems were calculated (details in the Supporting Information online and Tables S3–S6) and the values for several representative samples are shown in Table S7.

It is noted that while this EID model is likely to be too simple and significant errors may be generated, we believe that this is workable and the obtained trend should be reliable since the solvent molecules around the electrolyte ion are believed to be tightly absorbed and should be most likely carried by the ions. This approach has also been used in the literature for electrolyte ion solvation studies [32–35].

3.3 Experimental capacitance and its relationship with E-SSA

Now we come to study the experimental capacitance C_{ex} of these bulk sp^2 carbon materials. The C_{ex} values of SCs for various sp^2 carbon materials were obtained following the recommended method [21,23], as shown in Table S8. In our previous studies, it was found that in IL electrolytes ($EMIMBF_4$ and $BMIMBF_4$), C_{ex} is linearly dependent on E-SSA [31]. It would thus be important to know the

generality of this linear dependence in other electrolyte systems, such as organic and aqueous systems, which are widely used in state-of-the-art industrial SC systems.

With the numerous experimental data available, it is surprising to find that this linear relationship is much more general and can be applied to all the studied electrolyte systems. Examples of this linear relationship between C_{ex} and E-SSA are shown in Figure 1(a–g). First, as shown in Figure 1(a–d), for the same electrolyte system, a clear linear dependence of C_{ex} on the E-SSA of different carbon materials is observed for all systems. In addition, a linear relationship was also observed when C_{ex} was plotted against E-SSA for the same material but in different electrolyte systems, as shown in Figure 1(e–g). The different EIDs of the studied electrolyte ions lead to different E-SSAs for the same carbon material in different electrolyte systems. Note that different capacitances were observed for the same E-SSA when the same electrolyte was used but with different solvents, such as for RP20 in $TEABF_4$/AN and in $TEABF_4$/PC (Figure 1(e)). This is due to the different dielectric constants and the thicknesses of the electric double layer (d) of the two electrolyte systems. A linear relationship between C_{ex} and E-SSA also exists for the carbon materials in all the electrolyte systems studied. Furthermore, the numerical values of all the slopes in Figure 1(a–g) are very similar. So if the above data are all plotted together, there is a general linear relationship between C_{ex} and E-SSA described by the linear equation Y=0.126X–3.62 for all the materials in all the electrolyte systems, as shown in Figure 1(h). While the reason and its implication for this general linear relationship is yet to be understood, it implies that with a given carbon material and electrolyte system, the capacitance can be estimated directly and reliably without fabricating the devices.

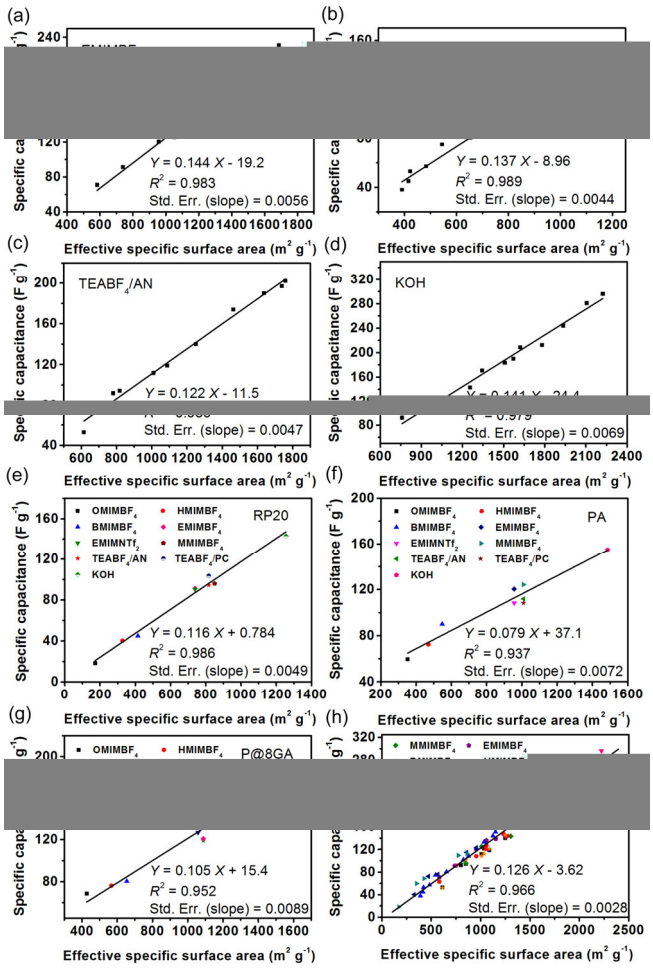

Figure 1 The relationship between C_{ex} and E-SSA for various sp^2 carbon materials. Materials in the same electrolyte system (a) $EMIMBF_4$, (b) $BMIMBF_4$, (c) $TEABF_4$/AN and (d) KOH. The same material in different electrolyte systems (e) RP20, (f) PA and (g) P@8GA. (h) General relationship for all studied sp^2 carbon materials in different electrolyte systems.

3.4 Direct comparison of experimental and theoretical capacitance

Using the EID model, the calculated theoretical specific capacitances and the experimental values, as shown in Figures 2 and S2, give a surprisingly good agreement for all the carbon materials in different electrolyte systems studied. For example, in the $EMIMBF_4$ system, the C_{th} values for P@16GA, S@24GA, GAC, P@8GA and RP20 are 216, 209, 139, 129 and 96 F g^{-1} respectively and these are generally consistent with the respective C_{ex} values of 231, 216, 139, 136 and 91 F g^{-1}. For S@24GA, the C_{th} values are 209, 198 and 278 F g^{-1} in $EMIMBF_4$, $TEABF_4$/AN and KOH systems, respectively, corresponding to C_{ex} values of 216, 197 and 281 F g^{-1}. The highest theoretical C_{th} of 290 F g^{-1} was obtained for P@16GA in KOH, which is consistent with the experimental value of 296 F g^{-1}.

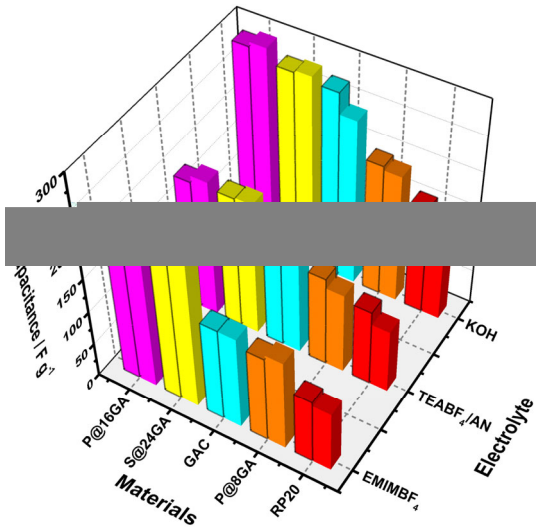

Figure 2 The relationship between C_{ex} and C_{th} of several representative carbon materials in $EMIMBF_4$, $TEABF_4$/AN and KOH electrolyte systems. In each pair of the columns, the one with bolder black border is C_{th} and the other is C_{ex}.

The consistency between the experimental and theoretical values indicates that the EID model for the calculation of theoretical specific capacitance is appropriate for SCs for all the systems studied.

3.5 Theoretical investigation for possible highest SSA of bulk sp^2 carbon materials in practice

While various experimental approaches have been tried to obtain the material with the highest possible SSA, our best experimental result obtained is about 3500 $m^2\ g^{-1}$, as discussed above. The remaining important question is what is the theoretical limit for the best SSA. Note that the best reported experimental SSA may not be the best in practice, since it is possible the optimum processing parameters to make such a material were not achieved in our experiments. The theoretical approach was therefore used to search for such a limit.

Our approach is based on the following assumptions: (1) all the bulk sp^2 carbon materials have graphene sheets as the basic building block [36,37], though there may be differences in terms of sheet size, stacking, defects and so on; (2) the extra surface area above the theoretical limit of 2630 $m^2\ g^{-1}$ of graphene comes mainly from the edge contribution of the graphene sheets [16,38,39]. So under similar conditions, materials consisting of smaller graphene sheets should have higher edge contribution and SSA values. It is also important to note that to have the possible highest surface area, the graphene sheets need to be single-layer [16,40].

With these assumptions, the key to answer the proposed question about the best SSA of bulk sp^2 carbon material is what is the smallest (average) size of graphene sheets in the bulk after undergoing harsh chemical treatment such as KOH treatment at 900 °C. It is important to note that in theory there is a limit for the smallest sheet that can be obtained (thermodynamically stable) during the process. This is because when the sheet size gets too small, the graphene sheets (behaving as a large fused polyaromatic compound) tend to be less stable and will react with each other to form a large graphene sheet (larger polyaromatic compound) [41].

So if the size of the smallest stable graphene sheet under practical conditions, such as at 900 °C, is obtained, the highest SSA of sp^2 carbon materials would be obtained by assuming all the graphene sheets are single-layer. To achieve this goal, a series of thermodynamic calculations were carried out using DFT calculation. We hypothesize that the easiest reaction, due to the instability of a small graphene sheet (fragment) to reduce the corresponding surface area, is its dimerization, as defined in Eq. (2):

$$\text{Ar–H (s)+Ar–H (s)} \rightarrow \text{Ar–Ar (s)+}H_2\text{(g)} \qquad (2)$$

where Ar represents benzene, naphathlene, phenanthrene, anthracene, pyrene, coronene and different sized graphene fragments, where the graphene fragments have lateral sizes of 0.5 nm×0.5 nm, 1.0 nm×1.0 nm, 1.5 nm×1.5 nm, 2.0 nm×2.0 nm and 2.5 nm×2.5 nm, respectively, which are respectively denoted graphene 0505, graphene 1010, graphene 1515, graphene 2020 and graphene 2525.

According to the laws of thermodynamics, if the Gibbs free energy change $\Delta_r G$ of this reaction is negative at a given temperature, the reaction should happen spontaneously so that the graphene fragment is unstable and larger graphene sheets should be formed. Therefore $\Delta_r G$ of this reaction for a series of graphene sheets (fragments) with different sizes from the smallest benzene to a graphene sheet with the lateral size of 2.5 nm×2.5 nm (~252 carbon atoms) was calculated for 900 °C, which is the most widely used temperature in the activation step for the production of ACs in both academic laboratories and industry. Note that the geometric optimization of larger graphene sheets was limited by our computing power, so an extrapolation was used. The details of the DFT modeling and the thermodynamic calculations are given in the Supporting Information online.

Obviously, it is more reasonable to use Gibbs free energy change of the reaction per carbon atom, $\Delta_r G/n$, to represent the spontaneous driving force to avoid the size effect. As can be seen from the $\Delta_r G/n$ results (Table S9), the smallest fragment (benzene unit) has the most negative $\Delta_r G$, indicating it would have a rather high spontaneous driving force to form a larger fragment, as expected. As the size gets larger, the driving force gets smaller, which is consistent with the less negative $\Delta_r G/n$ shown in Table S9. By plotting $\Delta_r G/n$ values against the size (number of carbon atoms) of the graphene sheets, as shown in Figure 3(a), we can see that with increasing number of carbon atoms, $\Delta_r G/n$ has a rather large initial negative value and becomes less negative and approaches zero, consistent with the intuitive understanding of chemistry [42]. To mathematically predict where $\Delta_r G/n$ actually reaches zero, a plot of $\Delta_r G/n$ versus $1/n$ is shown in Figure 3(b) and this plot gives a linear relationship with a correlation coefficient R^2=0.995. The extrapolation of this linear fit shows that when the carbon atom number reaches ~1322, $\Delta_r G/n$ is zero. If we simply use the simplest square shape for the smallest graphene obtained above, the size would be about 5×5–6×6 nm^2, corresponding to a theoretical SSA of ~3500–3700 $m^2\ g^{-1}$ based on a calculation model

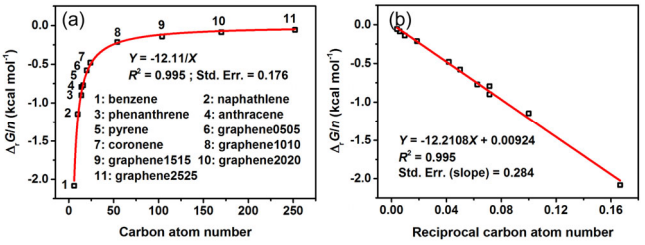

Figure 3 $\Delta_r G/n$ at 900 °C with (a) the number of carbon atoms and (b) the reciprocal of the number of carbon atoms.

(Supporting Information online).

We can now estimate the best practical capacitance for the highest possible SSA. If we assume all the SSA is used (E-SSA=100% SSA), the possible C_{th} for different electrolyte systems can be estimated, as summarized in Table S10. For example, the best C_{th} obtained was 485–514 F g^{-1} for the $EMIMBF_4$ system which has the largest dielectric constant of the four widely used electrolyte systems. These results indicate that these is still some room for improvement in the capacitance performance obtained in practice. This probably requires optimization of the pore size control which could be different for different electrolyte systems.

4 Conclusions

In summary, a systematic investigation has been carried out both experimentally and theoretically to obtain the highest specific surface area and the best capacitance performance of the bulk sp^2 carbon materials for SC applications. It is found that the possible limit for such surface area is around 3500–3700 m^2 g^{-1}. This corresponds to a best capacitance performance in the range of 485–514 F g^{-1} for one of the most widely used electrolytes, $EMIMBF_4$, due to its high dielectric constant. If control/optimization of the morphology of bulk sp^2 carbon materials could be achieved, a higher capacitance performance for SC should be obtained. Also, the general linear relationship between experimental capacitance and the E-SSA of different sp^2 carbon materials in different electrolyte systems could be used to easily and reliably evaluate the capacitance performance of sp^2 carbon materials without tedious and sometimes inaccessible device fabrication. This should speed up the material design and screening.

Supporting information

The supporting information is available online at chem.scichina.com and link.springer.com/journal/11426. The supporting materials are published as submitted, without typesetting or editing. The responsibility for scientific accuracy and content remains entirely with the authors.

This work was supported by the National Basic Research Program of China (2012CB933401), the National Natural Science Foundation of China (51472124, 51273093, 21374050), the Natural Science Foundation of Tianjin (13RCGFGX01121) and Science Research Project of Langfang Teachers University (LSLB201401).

1 Simon P, Gogotsi Y. Capacitive energy storage in nanostructured carbon-electrolyte systems. *Acc Chem Res*, 2012, 46: 1094–1103
2 Zhang LL, Zhao XS. Carbon-based materials as supercapacitor electrodes. *Chem Soc Rev*, 2009, 38: 2520–2531
3 Yang S, Bachman RE, Feng X, Müllen K. Use of organic precursors and graphenes in the controlled synthesis of carbon-containing nanomaterials for energy storage and conversion. *Acc Chem Res*, 2012, 46: 116–128
4 Zhai Y, Dou Y, Zhao D, Fulvio PF, Mayes RT, Dai S. Carbon materials for chemical capacitive energy storage. *Adv Mater*, 2011, 23: 4828–4850
5 Ghosh A, Lee YH. Carbon-based electrochemical capacitors. *ChemSusChem*, 2012, 5: 480–499
6 Zhu J, Yang D, Yin Z, Yan Q, Zhang H. Graphene and graphene-based materials for energy storage applications. *Small*, 2014, 10: 3480–3498
7 Largeot C, Portet C, Chmiola J, Taberna PL, Gogotsi Y, Simon P. Relation between the ion size and pore size for an electric double-layer capacitor. *J Am Chem Soc*, 2008, 130: 2730–2731
8 Wu ZS, Sun Y, Tan YZ, Yang SB, Feng XL, Müllen K. Three-dimensional graphene-based macro- and mesoporous frameworks for high-performance electrochemical capacitive energy storage. *J Am Chem Soc*, 2012, 134: 19532–19535
9 Qie L, Chen W, Xu H, Xiong X, Jiang Y, Zou F, Hu X, Xin Y, Zhang Z, Huang Y. Synthesis of functionalized 3d hierarchical porous carbon for high-performance supercapacitors. *Energy Environ Sci*, 2013, 6: 2497–2504
10 Wen Z, Wang X, Mao S, Bo Z, Kim H, Cui S, Lu G, Feng X, Chen J. Crumpled nitrogen-doped graphene nanosheets with ultrahigh pore volume for high-performance supercapacitor. *Adv Mater*, 2012, 24: 5610–5616
11 Wang DW, Li F, Liu M, Lu GQ, Cheng HM. 3D Aperiodic hierarchical porous graphitic carbon material for high-rate electrochemical capacitive energy storage. *Angew Chem Int Ed*, 2008, 47: 373–376
12 Xu Y, Sheng K, Li C, Shi G. Self-assembled graphene hydrogel via a one-step hydrothermal process. *ACS Nano*, 2010, 4: 4324–4330
13 Chen J, Li C, Shi G. Graphene materials for electrochemical capacitors. *J Phys Chem Lett*, 2013, 4: 1244–1253
14 Biswal M, Banerjee A, Deo M, Oqale S. From dead leaves to high energy density supercapacitors. *Energy Environ Sci*, 2013, 6: 1249–1259
15 Zhang F, Zhang T, Yang X, Zhang L, Leng K, Huang Y, Chen Y. A high-performance supercapacitor-battery hybrid energy storage device based on graphene-enhanced electrode materials with ultrahigh energy density. *Energy Environ Sci*, 2013, 6: 1623–1632
16 Zhang L, Zhang F, Yang X, Long G, Wu Y, Zhang T, Leng K, Huang Y, Ma Y, Yu A, Chen Y. Porous 3D graphene-based bulk materials with exceptional high surface area and excellent conductivity for supercapacitors. *Sci Rep*, 2013, 3: 1408
17 Wei L, Sevilla M, Fuertes AB, Mokaya R, Yushin G. Hydrothermal carbonization of abundant renewable natural organic chemicals for high-performance supercapacitor electrodes. *Adv Energy Mater*, 2011, 1: 356–361
18 Zhu Y, Murali S, Stoller MD, Ganesh KJ, Cai W, Ferreira PJ, Pirkle A, Wallace RM, Cychosz KA, Thommes M, Su D, Stach EA, Ruoff RS. Carbon-based supercapacitors produced by activation of graphene. *Science*, 2011, 332: 1537–1541
19 Lu Y, Zhang F, Zhang T, Leng K, Zhang L, Yang X, Ma Y, Huang Y, Zhang M, Chen Y. Synthesis and supercapacitor performance studies of *N*-doped graphene materials using *o*-phenylenediamine as the double-*N* precursor. *Carbon*, 2013, 63: 508–516
20 Wang Y, Shi Z, Huang Y, Ma Y, Wang C, Chen M, Chen Y. Supercapacitor devices based on graphene materials. *J Phys Chem C*, 2009, 113: 13103–13107
21 Stoller MD, Park S, Zhu Y, An J, Ruoff RS. Graphene-based ultracapacitors. *Nano Lett*, 2008, 8: 3498–3502
22 Stoller MD, Ruoff RS. Best practice methods for determining an electrode material's performance for ultracapacitors. *Energy Environ Sci*, 2010, 3: 1294–1301
23 Gogotsi Y, Simon P. True performance metrics in electrochemical energy storage. *Science*, 2011, 334: 917–918
24 Becke AD. Density-functional thermochemistry. III. The role of exact exchange. *J Chem Phys*, 1993, 98: 5648–5652
25 Lee C, Yang W, Parr RG. Development of the colle-salvetti correlation-energy formula into a functional of the electron density. *Phys Rev B*, 1988, 37: 785–789
26 Israelachvili JN. *Intermolecular and Surface Forces*. 3rd ed. USA: Academic Press, 2011. 79

27 Volkov AG, Paula S, Deamer DW. Two mechanisms of permeation of small neutral molecules and hydrated ions across phospholipid bilayers. *Bioelectrochem Bioenerg*, 1997, 42: 153–160

28 Huang J, Sumpter BG, Meunier V. A universal model for nanoporous carbon supercapacitors applicable to diverse pore regimes, carbon materials, and electrolytes. *Chem-Eur J*, 2008, 14: 6614–6626

29 Dueren T, Millange F, Ferey G, Walton KS, Snurr RQ. Calculating geometric surface areas as a characterization tool for metal-organic frameworks. *J Phys Chem C*, 2007, 111: 15350–15356

30 Connolly ML. Solvent-accessible surfaces of proteins and nucleic acids. *Science,* 1983, 221: 709–713

31 Zhang L, Yang X, Zhang F, Long G, Zhang T, Leng K, Zhang Y, Huang U, Ma Y, Zhang M, Chen Y. Controlling the effective surface area and pore size distribution of sp^2 carbon materials and their impact on the capacitance performance of these materials. *J Am Chem Soc*, 2013, 135: 5921–5929

32 Lin R, Taberna PL, Chmiola J, Guay D, Gogotsi Y, Simon P. Microelectrode study of pore size, ion size, and solvent effects on the charge/discharge behavior of microporous carbons for electrical double-layer capacitors. *J Electrochem Soc*, 2009, 156: A7–A12

33 Feng G, Qiao R, Huang J, Sumpter BG, Meunier V. Ion distribution in electrified micropores and its role in the anomalous enhancement of capacitance. *ACS Nano*, 2010, 4: 2382–2390

34 Jiang DE, Jin Z, Henderson D, Wu JZ. Solvent effect on the pore-size dependence of an organic electrolyte supercapacitor. *J Phys Chem Lett*, 2012, 3: 1727–1731

35 Huang J, Sumpter BG, Meunier V. Theoretical model for nanoporous carbon supercapacitors. *Angew Chem Int Ed*, 2008, 47: 520–524

36 Dahn JR, Zheng T, Liu Y, Xue JS. Mechanisms for lithium insertion in carbonaceous materials. *Science*, 1995, 270: 590–593

37 Pré P, Huchet G, Jeulin D, Rouzaud JN, Sennour M, Thorel A. A new approach to characterize the nanostructure of activated carbons from mathematical morphology applied to high resolution transmission electron microscopy images. *Carbon*, 2013, 52: 239–258

38 Chae HK, Siberio-Perez DY, Kim J, Go YB, Eddaoudi M, Matzger AJ, O'Keeffe M, Yaghi OM. A route to high surface area, porosity and inclusion of large molecules in crystals. *Nature*, 2004, 427: 523–527

39 Sarkisov L. Accessible surface area of porous materials: understanding theoretical limits. *Adv Mater*, 2012, 24: 3130–3133

40 Kaneko K, Ishii C, Ruike M, Kuwabara H. Origin of superhigh surface area and microcrystalline graphitic structures of activated carbons. *Carbon*, 1992, 30: 1075–1088

41 Barone V, Hod O, Scuseria GE. Electronic structure and stability of semiconducting graphene nanoribbons. *Nano Lett*, 2006, 6: 2748–2754

42 Barnard AS, Snook IK. Thermal stability of graphene edge structure and graphene nanoflakes. *J Chem Phys*, 2008, 128: 094707